Discrete Wavelet Analysis: A New Framework for Fast Optic Flow Computation

Christophe P. Bernard

Centre de Mathématiques Appliquées
École Polytechnique
91128 Palaiseau cedex, France
bernard@cmapx.polytechnique.fr

Abstract. This paper describes a new way to compute the optical flow based on a discrete wavelet basis analysis. This approach has thus a low complexity ($O(N)$ if one image of the sequence has N pixels) and opens the way to efficient and unexpensive optical flow computation. Features of this algorithm include multiscale treatment of time aliasing and estimation of illumination changes.

Keywords Analytic wavelets, Image compression, Optic flow, Illumination, Discrete wavelets.

1 Introduction

Optic flow detection consists in computing the motion field $\mathbf{v} = (v_1, v_2)$ of the features of an image sequence in the image plane. Applications range from moving image compression to real scene analysis and robotics.

Given an image sequence $I_t(x_1, x_2)$ we want to measure the optical flow $\mathbf{v} = (v_1, v_2)$ that matches the well known *optical flow equation*

$$I_{t+\delta t}(x_1 + v_1\delta t, x_2 + v_2\delta t) = I_t(x_1, x_2) \ , \tag{1}$$

or its differential counterpart

$$\frac{\partial I_t}{\partial x_1}v_1 + \frac{\partial I_t}{\partial x_2}v_2 + \frac{\partial I_t}{\partial t} = 0 \ . \tag{2}$$

No point-wise resolution of (2) is possible, since on each location and each time, this would consist in solving a single scalar equation for two scalar unknowns. This is the *aperture problem.*

1.1 Previous Work

Horn & Schunck [13] [14] wrote a pioneering paper on the subject in 1980. Then, several methods where proposed: region matching methods [2], differential methods [16] and spatiotemporal filtering methods [1] [6] [9] [11] [12], on

which Barron *& al.* made an extensive review [3]. Later, Burns *& al.* developed a discrete wavelet spatiotemporal filtering technique [4], and Weber & Malik designed a filtered differential method [21].

In this profusion of methods, two points always arise:

Additional assumption The only way to get rid of aperture is to do an additional assumption on the optic flow, expressed or implied. Horn & Schunck minimize a smoothness functional; region based matching methods, and filtering based methods [2] [1] [6] [9] [11] [12] [4] [21] rely explicitly on the assumption that the optic flow is constant over quadrangular domains.

Multiscale approach Because of *time aliasing*, the optic flow measurement must be performed on a multi-scale basis. Coarse scales for detection of large displacements and finer scales for smaller displacements.

1.2 Motivation

This work was motivated by the belief that wavelet bases, as described by Ingrid Daubechies [7] Stéphane Mallat [17] are a very well designed tool for our purpose for several reasons:

- Wavelet bases have a natural multiscale structure;
- As a local frequency analysis tool, wavelet analysis compares favorably to filtering (as used in [1] [6] [9] [11] [12] [21]) because it is far less computation intensive, and still provides a complete information on this signal;
- With the additional assumption that the optic flow is locally constant, they provide an easy way to solve the aperture problem.

1.3 Road Map

In Sect. 2, we show how we solve the aperture problem. Section 3 is devoted to numerical experimentation. Time aliasing problems are addressed in Sect. 4, and Sect. 5–6 respectively focus on stability enhancement with analytic wavelets, and to the design of dyadic filter bank wavelets that are specific to the optic flow measurement, and are a key point in achieving these measurements in a short time.

2 Suggested Solution

2.1 Wavelet Notations

We start from a set of mother wavelets $(\psi^s)_{s=1\ldots S}$ in $L_2(\mathbb{R}^2)$. We then define a discrete wavelet family $(\psi^s_{j\mathbf{k}})_{s=1\ldots S, j\in\mathbb{Z}, \mathbf{k}\in\mathbb{Z}^2}$ by

$$\psi^s_{j\mathbf{k}}(\mathbf{x}) = 2^j \psi^s(2^j\mathbf{x} - \mathbf{k})$$

where j is a resolution index and $\mathbf{k} = (k_1, k_2)$ a 2-dimensional translation index, and $\mathbf{x}$ a 2–dimensional variable $\mathbf{x} = (x_1, x_2)$.

EXAMPLE —In image processing, a set of three mother wavelets is commonly used. These wavelets are built as tensor products of a scaling function $\phi \in L_2(\mathbb{R})$ and a wavelet $\psi \in L_2(\mathbb{R})$:

$$\psi^1(\mathbf{x}) = \psi(x_1)\phi(x_2) \tag{3}$$
$$\psi^2(\mathbf{x}) = \phi(x_1)\psi(x_2) \tag{4}$$
$$\psi^3(\mathbf{x}) = \psi(x_1)\psi(x_2) \tag{5}$$

Note that a wavelet $\psi^s_{j\mathbf{k}}$ is located around $(2^{-j}k_1, 2^{-j}k_2)$, and spreads over domain of size proportional to 2^{-j}.

2.2 Local Systems

Given such a basis, we do an inner product of (2) with all the S different wavelets that we have at scale j and location $\mathbf{k}$, getting thus S different equations.

$$\iint \left(\frac{\partial I_t}{\partial x_1} v_1(\mathbf{x}) + \frac{\partial I_t}{\partial x_2} v_2(\mathbf{x}) + \frac{\partial I_t}{\partial t} \right) \psi^s_{j\mathbf{k}}(\mathbf{x}) dx_1 dx_2 = 0 \qquad \forall s = 1 \dots S \tag{6}$$

Using the notation $< f, g >= \iint f(\mathbf{x}) g(\mathbf{x}) dx_1 dx_2$, this can also be written as

$$\left\langle \frac{\partial I_t}{\partial x_1} v_1, \psi^s_{j\mathbf{k}} \right\rangle + \left\langle \frac{\partial I_t}{\partial x_2} v_2, \psi^s_{j\mathbf{k}} \right\rangle + \left\langle \frac{\partial I_t}{\partial t}, \psi^s_{j\mathbf{k}} \right\rangle = 0 \qquad \forall s = 1 \dots S \tag{7}$$

For a given resolution j and translation index $\mathbf{k}$, we do the following assumption:

($\mathcal{A}_{j\mathbf{k}}$): $v_1(\mathbf{x})$ *and* $v_2(\mathbf{x})$ *are constant over* support$^1(\psi^s_{j\mathbf{k}})$ *for all* $s = 1..S$

Equation (7) then becomes

$$\left\langle \frac{\partial I_t}{\partial x_1}, \psi^s_{j\mathbf{k}} \right\rangle v_1 + \left\langle \frac{\partial I_t}{\partial x_2}, \psi^s_{j\mathbf{k}} \right\rangle v_2 + \frac{\partial}{\partial t} \left\langle I_t, \psi^s_{j\mathbf{k}} \right\rangle = 0 \qquad \forall s = 1 \dots S$$

and after an integration by parts

$$\boxed{\left\langle I_t, \frac{\partial \psi^s_{j\mathbf{k}}}{\partial x_1} \right\rangle v_1 + \left\langle I_t, \frac{\partial \psi^s_{j\mathbf{k}}}{\partial x_2} \right\rangle v_2 = \frac{\partial}{\partial t} \left\langle I_t, \psi^s_{j\mathbf{k}} \right\rangle} \qquad \forall s = 1 \dots S \ . \tag{8}$$

For j and $\mathbf{k}$ fixed, we have a *local system* of 3 equations with 2 unknowns v_1 and v_2, that has to be compared to the single equation (2): now we have found a way around aperture.

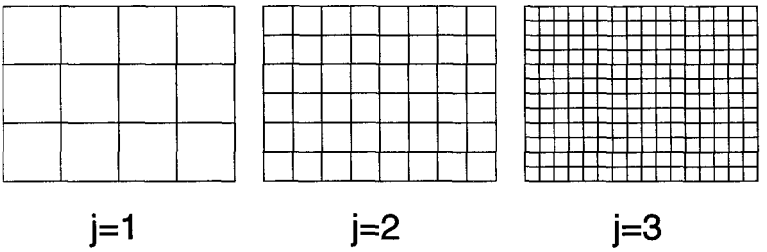

Fig. 1. Measure grids at several scales

2.3 Solving the Local Systems

For some scale indexes $j = 1, 2, 3$, the corresponding discrete grids $\{2^{-j}(k_1, k_2)\}$ are displayed in Fig. 1. At each node of each of these, we have a local system (8).

A question arises: what grid should we choose for our optic flow measurement? The answer depends on several factors.

— Arguments towards finer scale grids are (1) that we get a finer knowledge of the space dependence of the optic flow and (2) that the needed assumptions on the optic flow $\mathcal{A}_{j\mathbf{k}}$ are looser when the scale is finer.

— However, there is a strong argument against going towards finer scales: time aliasing (see Sect. 4). Time aliasing limits reliable estimation of the flow at a given scale j to flows that are smaller than $\alpha 2^{-j}$, where α is some constant of $[0, 1/2)$.

2.4 Adaptive Choice of the Measure Scale

The time aliasing limitation making fine scale measurements unreliable, we will start with coarse scale measures and then refine our measure. The behavior of a local system at a given scale j and location $2^{-j}(k_1, k_2)$ hints us whether at a given location, we stick at the current scale, or we use finer scale estimation.

1. If the system has a unique solution (v_1, v_2), we get a straightforward estimation of the optic flow at $2^{-j}\mathbf{k}$. Thus the measure scale j is suitable.
2. If the system has no solution, it means that our assumption $\mathcal{A}_{j\mathbf{k}}$ is incorrect. In such a case, we try to do finer scale measurements, since they rely on looser assumptions $\mathcal{A}_{j+1,\mathbf{k}'}$.

   If for example our measure region overlaps two regions where the flow is different, we have to split our measure region in subregions, to perform again this measure on each of these subregions, where hopefully the optic flow is locally constant.

[1] For the simplicity of our statement, we will consider the interval where most of the $L_2(\mathbb{R})$–energy of the wavelets is concentrated, and suppose that this support is $2^{-j}\mathbf{k} + [-2^{-j-1}; 2^{-j-1}]^2$.

3. If on the contrary, the system has infinitely many solutions, this means that the pattern at the location we are looking at is too poor to tell us how it is moving. The aperture problem remains.
   A typical case is a locally translation invariant pattern, because then it is impossible to measure its translation along his translation invariance axis.

As a safeguard against errors induced by time aliasing, we add two tests. The first is done in case 1, where we reject measures (v_1, v_2) that are above the time aliasing threshold (ie $|(v_1, v_2)| > \alpha \times 2^{-j}$). The second is done in case 2, where we make a least-squares estimate of $\mathbf{v}$. If $|\mathbf{v}| > \alpha \times 2^{-j-1}$, we give up any estimation at that location, since even finer scale estimations are false because of aliasing.

3 Numerical Experimentation

The algorithm was implemented with a dedicated set of *analytic* mother wavelets. The motivation of their use as well as their construction are described in Sect. 5.

3.1 True Sequences

Image sequences were downloaded from Barron *& al.*'s FTP site at *csd.uwo.ca*. The algorithm was tested on the rubik sequence (a rubik's cube on a rotating plate), the taxi sequence (where three vehicles are moving respectively towards East, West and Northwest) and the NASA sequence, which a is zoom on a Coke can.

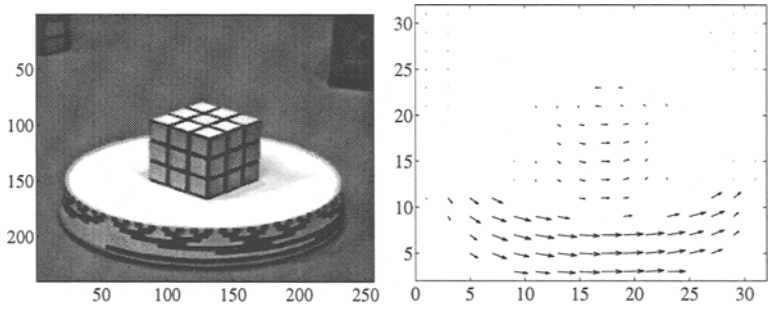

Fig. 2. Rubik sequence and flow

3.2 Synthetic Sequences

The described algorithm was also run on classical synthetic sequences (including Yosemite), and the result was compared to classical methods (Heeger, Fleet &

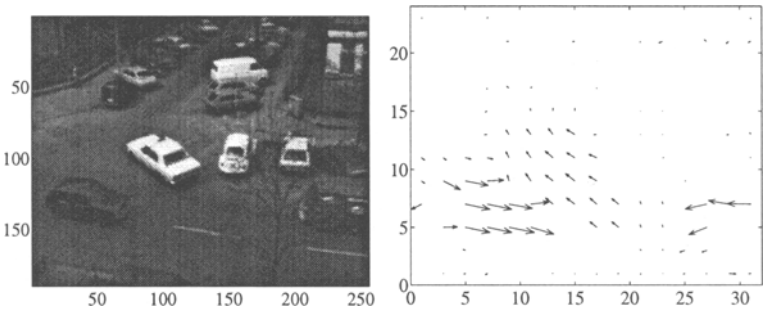

Fig. 3. Taxi sequence

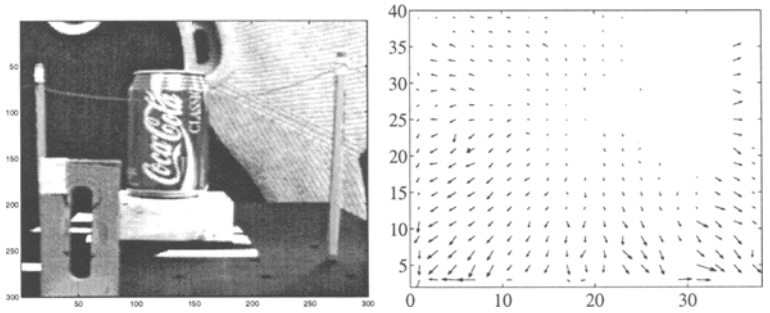

Fig. 4. NASA sequence

Jepson, Weber & Malik). The estimations errors are about 1.2 times higher, and are thus a little weaker. Reasons for this are that

- the suggested method is a two-frame method, while others rely on a number of frames ranging from 10 to 64;
- there no is coarse scale oversampling, and no coarse scale error averaging. The small loss of accuracy induced by this is counterbalanced by a much lower computational cost.

3.3 Illumination Changes

We use a new optic flow equation

$$\frac{\partial I_t}{\partial x} v_x + \frac{\partial I_t}{\partial y} v_y + \frac{\partial I_t}{\partial t} = \lambda I_t$$

instead of (2) where $\lambda = \frac{\partial}{\partial t} \log L$ is the logarithmic derivative of the illumination factor L. We use an additional wavelet shape $\psi^0(x, y) = \phi(x)\phi(y)$ of nonzero integral, and perform illumination change measurements, that is, estimate the new unknown parameter λ.

A synthetic sequence (moving white noise, with increasing illumination of Gaussian shape) was created. Three pictures of the sequence (Fig. 5) and the corresponding measured flow and illumination map (Fig. 6) are displayed. The real optic flow is of $(1.2, 0.8)$ pixels per frame, and the average error in degrees as measured by Barron & al. is less than 1.

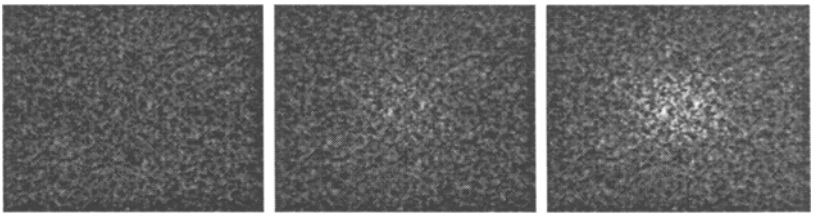

Fig. 5. Moving random pattern with varying illumination

4 Time Aliasing

Since our picture sequence is time sampled, the computation of the right–hand side coefficient in (8)

$$\frac{\partial}{\partial t}\langle I_t, \psi^s_{j\mathbf{k}}\rangle$$

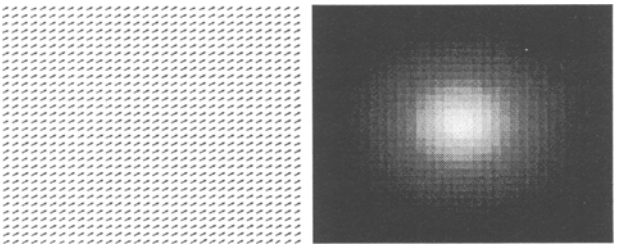

Fig. 6. Measured flow and illumination maps

relies on a finite difference approximation of the picture time derivative $\frac{\partial}{\partial t} I_t$ in time, like $\frac{\partial}{\partial t} I_t \simeq I_{t+1} - I_t$. We will see that the error of such estimations is high if the displacement (v_1, v_2) between two pictures I_t and I_{t+1} is large with regard to the wavelet scale 2^{-j}.

Note that this phenomenon always arises in some form in optic flow computation and has been pointed out by many authors [15]. Also note that this very problem motivates a multiscale approach to optic flow computation [2] [4] [18] [21].

Let us suppose that for a given j and $\mathbf{k}$, the picture is translating uniformly over the support of our wavelets $\psi^s_{j\mathbf{k}}$ for all s, ie

$$I_t(\mathbf{x}) = I(\mathbf{x} - t\mathbf{v})$$

4.1 Error Bound

The simplest time derivative approximation is a two step finite difference

$$\frac{\partial I_t}{\partial t} \simeq I_{t+1} - I_t$$

In this paper however, we will use higher order estimate, and measure the optic at each $t + 1/2$, between two successive pictures, based on the following approximation:

$$\frac{\partial I_{t+1/2}}{\partial t} \simeq I_{t+1} - I_t$$

Now we also need to compute coefficients of the left hand side of (8) at $t + 1/2$: $< \frac{\partial}{\partial x_i}\psi^s_{j\mathbf{k}}, I_{t+1/2} >$, because we only know them at integer times. This is done with the following estimation:

$$\frac{\partial}{\partial t} I_{t+1/2} \simeq \frac{I_t + I_{t+1}}{2}$$

At a given resolution j, these approximations lead respectively to the following coefficient approximations:

$$< \frac{\partial I_{t+1/2}}{\partial t}, \psi_{j\mathbf{k}} > \simeq \langle I_{t+1} - I_t, \psi_{j\mathbf{k}} \rangle \tag{9}$$

$$< I_{t+1/2}, \psi_{j\mathbf{k}} > \simeq \left\langle \frac{I_{t+1} + I_t}{2}, \psi_j\mathbf{k} \right\rangle \tag{10}$$

which can be rewritten after variable changes and integrations by parts

$$< I_{t+1/2}, \mathbf{v}.\nabla\psi_{j\mathbf{k}} > \simeq \langle I_{t+1/2}, \psi_{j\mathbf{k}}(\mathbf{x} + \mathbf{v}/2) - \psi_{j\mathbf{k}}(\mathbf{x} - \mathbf{v}/2) \rangle \tag{11}$$

$$< I_{t+1/2}, \psi_{j\mathbf{k}} > \simeq \left\langle I_{t+1/2}, \frac{\psi_{j\mathbf{k}}(\mathbf{x} + \mathbf{v}/2) + \psi_{j\mathbf{k}}(\mathbf{x} - \mathbf{v}/2))}{2} \right\rangle \tag{12}$$

4.2 Design Rule

Each approximation (11) and (12) is the approximation of a linear functional of $L_2(\mathbb{R})$ with another one. We take as a design rule that the following approximations be true:

$$\mathbf{v}.\nabla\psi_{j\mathbf{k}} \simeq \psi_{j\mathbf{k}}(\mathbf{x}+\mathbf{v}/2) - \psi_{j\mathbf{k}}(\mathbf{x}-\mathbf{v}/2) \tag{13}$$

$$\psi_{j\mathbf{k}} \simeq \frac{\psi_{j\mathbf{k}}(\mathbf{x}+\mathbf{v}/2) + \psi_{j\mathbf{k}}(\mathbf{x}-\mathbf{v}/2))}{2} \tag{14}$$

With a Taylor expansion of ψ, we can prove that there exists some constant M such that the sum of the relative errors of (13) and (14) is less than $M \times (|\mathbf{v}|2^j)$. This sum has been numerically estimated for the wavelets we use later in this algorithm, and lead to the constraint

$$\boxed{|\mathbf{v}| \leq 0.42 \times 2^{-j}}$$

5 Analytic Wavelets

Standard real valued wavelets are displayed in Fig. (7–a-d). If we use wavelets ψ^1, ψ^2 and ψ^3 to compute the optic flow, the determinants of the system of equations (8) will be real valued and highly oscillating in space.

For these two reasons, they will vanish very often and make the flow estimation poor and unstable.

5.1 A Problem: Extinction

Going back to the one–dimensional case, we can write the velocity estimation as

$$v(k/2^j) \simeq \frac{\frac{\partial}{\partial t}\int I_t(x)\psi_{jk}(x)dx}{\int I_t(x)\psi'_{jk}(x)dx} \tag{15}$$

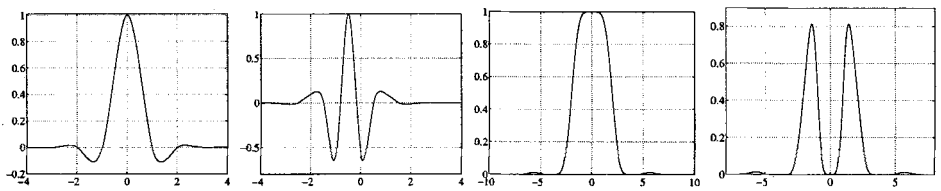

(a) ϕ (b) ψ (c) $|\hat{\phi}|$ (d) $|\hat{\psi}|$

Fig. 7. ϕ, ψ and their Fourier transforms

If ψ is a classical real-valued wavelet, as displayed in Fig. (7–a,c), its time and frequency behavior can be described with a local cosine model:

$$\psi(x) \simeq g(x)\cos(x) = \mathrm{Re}(g(x)e^{ix}) \tag{16}$$

where $g(x)$ is an even function with a frequency content significantly narrower that 2π. As a consequence, we can make the following approximation:

$$\psi'(x) = \mathrm{Re}(ig(x)e^{ix})$$

In this case, the denumerator of (15) is equal to

$$\begin{aligned} D(k/2^j) &= \mathrm{Re}\left(i2^j \int I_t(x) g(2^j x - k) e^{i(2^j x - k)} dx\right) \\ &= \mathrm{Re}\left(i2^j e^{-ik} \int I_t(x) e^{i2^j x} g(2^j x - k) dx\right) \\ &= \mathrm{Re}\left(ie^{-ik} \int I_t(2^{-j} y) e^{iy} g(y - k) dy\right) \qquad \text{by setting } y = 2^j x \end{aligned}$$

where the integral is a convolution C of two functions

$$\begin{gathered} y \mapsto I_t(y2^{-j})e^{iy} \\ \text{and } y \mapsto g(-y) = g(y) \end{gathered}$$

Because g has a narrow spectrum, so has C, and thus our denumerator is

$$D(k/2^j) = \mathrm{Re}(ie^{-ik}C(k))$$

where C is slowly varying. Therefore,

$$D(k/2^j) = \cos(k - \mathrm{Arg}\, C(k) + \pi/2) \times |C(k)| \tag{17}$$

where $\mathrm{Arg}(C(k))$ and $|C(k)|$ are slowly varying. The denumerator thus roughly behaves like a cosinus function. It is thus very likely to vanish or to be close to 0 for some k.

5.2 A Solution: Analytic Wavelets

If instead of this real valued wavelet ψ, we use its positive frequency analytic part ψ^+ defined as

$$\hat{\psi^+}(\xi) = 2 \times 1_{(\xi \geq 0)} \times \hat{\psi}(\xi)$$

equation (16) becomes

$$\psi(x) \simeq g(x)e^{ix}$$

that is the same formula now without the "real–part" operator. As a result, the cosine function is replaced by a complex exponential in (17) that becomes

$$D(k/2^j) = e^{i(k-\mathrm{Arg}\, C(k)+\pi/2)} \times |C(k)|$$

The modulus of $D(k/2^j)$ is now $|C(k)$ instead of $|\cos((k-\mathrm{Arg}\, C(k)+\pi/2)\times|C(k)|$ and is less often close to zero.

Two-dimension analytic wavelets This suggests us to replace our three real wavelets ψ^1, ψ^2 and ψ^3 as defined in equations (3–5), with the four following wavelets

$$\Psi^1(\mathbf{x}) = \psi^+(x_1)\phi(x_2) \tag{18}$$
$$\Psi^2(\mathbf{x}) = \phi(x_1)\psi^+(x_2) \tag{19}$$
$$\Psi^3(\mathbf{x}) = \psi^+(x_1)\psi^+(x_2) \tag{20}$$
$$\Psi^4(\mathbf{x}) = \psi^+(x_1)\psi^-(x_2) \tag{21}$$

where $\psi^-(t) = \overline{\psi^+(t)}$. It is easy to prove that if $(\psi^s_{j\mathbf{k}})_{s=1..3,j\in\mathbb{Z},\mathbf{k}\in\mathbb{Z}^2}$ is a basis of $L_2(\mathbb{R})$, then $(\Psi^s_{j\mathbf{k}})_{s=1..4,j\in\mathbb{Z},\mathbf{k}\in\mathbb{Z}^2}$ is a frame.

Analytic measure functions are also used in spatiotemporal filtering techniques, where velocity tuned filters are analytic [9]. Note, however, that the Hilbert transform is also used to make filters direction selective and not analytic [4] [20].

Psychophysical evidence also supports the use of analytic wavelets. Daugman [8] identified a pair of (real valued) Gabor filters with a $\pi/2$ phase shift between them

$$f_1 = e^{-(\mathbf{X}-\mathbf{X}_0)^2/2\sigma}\cos\mathbf{k}.\mathbf{X}$$
$$f_2 = e^{-(\mathbf{X}-\mathbf{X}_0)^2/2\sigma}\sin\mathbf{k}.\mathbf{X}$$

Such a pair can equivalently be seen as a single complex filter

$$f = e^{-(\mathbf{X}-\mathbf{X}_0)^2/2\sigma}e^{i\mathbf{k}.\mathbf{X}} \tag{22}$$

that now has a non-symmetric spectrum, and is thus an approximation of an analytic transform of f_1.

6 Dyadic Filter Bank Wavelets

For computational efficiency, we need wavelets implementable with dyadic filter banks, so that the computation of the system coefficients in (8) can be done with a fast wavelet transform. We will use separable wavelets $\psi(x_1, x_2) = f(x_1)g(x_2)$, and can therefore limit ourselves to the one-dimensional case.

Wavelet coefficients in the one–dimensional case can be computed with a dyadic pyramid filtering and subsampling scheme when the wavelet is an infinite convolution of discrete FIR[2] filters, which can be written in Fourier domain as

[2] finite impulse response

$$\hat{\psi}(\xi) = \prod_{j=1}^{+\infty} m_j\left(\frac{\xi}{2^j}\right) \tag{23}$$

where the m_j's are trigonometric polynomials. For computational efficiency purposes, the functions m_j should be all the same, up to the very first ones.

There exist plenty of dyadic filter bank wavelets. More difficult points are the computation of wavelet derivative coefficients also with dyadic filter banks, as well as the design of *analytic* dyadic filter bank wavelets.

6.1 Dyadic Filter Bank Wavelet Derivatives

If a function ψ is an infinite convolution of discrete filters

$$\hat{\psi}(\xi) = \prod_{j=1}^{+\infty} m_j\left(\frac{\xi}{2^j}\right)$$

then

$$\widehat{\psi'}(\xi) = \prod_{j=1}^{+\infty} m'_j\left(\frac{\xi}{2^j}\right)$$

where

$$m'_j(\xi) = \begin{cases} \frac{2m_j(\xi)}{e^{i\xi}+1} & \text{if } j \geq 2 \\ 2(e^{i\xi}-1)m_1(\xi) & \text{if } j = 1 \end{cases}$$

Proof. Thanks to the following identity

$$\prod_{j=1}^{+\infty} \frac{e^{i\xi/2^j}+1}{2} = \frac{e^{i\xi}-1}{i\xi}$$

we get,

$$\prod_{j=1}^{+\infty} m'_j\left(\frac{\xi}{2^j}\right) = i\xi \prod_{j=1}^{+\infty} m_j\left(\frac{\xi}{2^j}\right) = \widehat{\psi'}(\xi)$$

This shows that the derivative a dyadic filter bank wavelet is also implementable with a filter bank and gives us the rule to find the corresponding coefficients. The extension to partial derivatives of two–dimensional wavelets is straightforward.

6.2 Analytic Dyadic Filter Bank Wavelets

Using a true Hilbert transform to compute analytic wavelet coefficients is not possible in practice because of its computational cost. The purpose of this section is thus to approximate the Hilbert transform ψ^+ of a real wavelet ψ with an almost analytic wavelet $\psi^{\#}$ that can still be implemented with a FIR^2 filter bank.

We want our wavelet $\psi^{\#}$ to have most of its energy on the positive frequency peak, and we want to keep the relationship $\psi = 2\,\mathrm{Re}(\psi^{\#})$, the same way as for the true Hilbert transform, $\psi = 2\,\mathrm{Re}(\psi^{+})$.

Starting from any FIR filter pair m_0 and m_1 defining a wavelet as

$$\hat{\psi}(\xi) = m_1\left(\frac{\xi}{2}\right)\prod_{j=2}^{+\infty} m_0\left(\frac{\xi}{2^j}\right) \tag{24}$$

ψ and its Fourier transform are displayed in (7–a,b).

If m_2 is a Deslauriers-Dubuc interpolation filter, then $\hat{\psi}^{\#}(\xi) = \hat{\psi}(\xi)m_2(\xi/2 - \pi/4)$ is a good approximation of $\hat{\psi}^{+}(\xi)$, since most of the negative frequency peak of ψ is canceled by a vanishing $m_2(\xi)$. $\hat{\psi}$ (solid) and $m_2(\xi - \pi/4)$ (dashed) are displayed together in 8–a, and the resulting $\widehat{\psi^{\#}}$ in 8–b. The remaining negative frequency content of $\psi^{\#}$ is not 0, but is less than 2% of $\psi^{\#}$'s total L_2 norm. Also we have the relationship $\psi = 2\,\mathrm{Re}(\psi^{\#})$, because

$$m_2(\xi) + m_2(\xi + \pi) = 1 \quad \text{and} \quad m_2(\xi) = m_2(-\xi) \quad \forall \xi$$

Thanks to the way $\psi^{\#}$ is defined, inner products $\int I(x)\psi^{\#}(x)dx$ are computed the same way as $\int I(x)\psi(x)dx$ up to a single additional discrete filtering step.

Conclusion

The method presented in this paper is an improvement of the existing ones in terms of reduced computational complexity. This reduction is gained because

- the optic flow is computed with only two frames.
- the pyramid filtering and subsampling scheme structure allows to measure displacements at several scales without massive convolutions. As a consequence, optic flow of a standard sequence can be computed on a single processor computer in few seconds.

Acknowledgments

The author would like to express his gratefulness to Stéphane Mallat for very helpful comments and discussions and Jean-Jacques Slotine for stimulating discussions on possible applications in robotics.

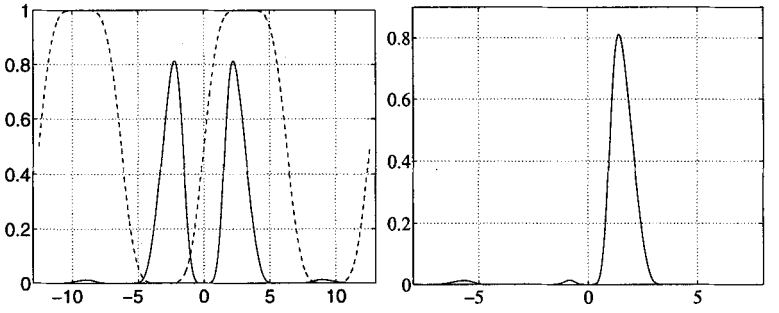

(a) $\hat{\psi}$ and $m_2(\frac{\xi}{2} - \frac{\pi}{4})$ (b) $|\widehat{\psi^{\#}}|$

Fig. 8. Approximation $\psi^{\#}$ of ψ^{+} and its Fourier transform

References

1. E. H. Adelson and J. R. Bergen, "Spatiotemporal Energy Models for the Perception of Vision," *J. Opt. Soc. Amer.*, Vol A2, pp. 284-299, 1985.
2. P. Anandan, "A Computational Framework and an Algorithm for the Measurement of Visual Motion," *International Journal of Computer Vision*, Vol. 2, pp. 283-310, 1989.
3. J.L. Barron, D.J. Fleet and S.S. Beauchemin, "Performance of Optical Flow Techniques," *International Journal of Computer Vision*, Vol. 12:1, pp. 43-77, 1994.
4. T.J. Burns, S.K. Rogers, D.W. Ruck and M.E. Oxley, "Discrete, Spatiotemporal, Wavelet Multiresolution Analysis Method for Computing Optical Flow," *Optical Engineering*, Vol. 33:7, pp. 2236-2247, 1994.
5. P.J. Burt and E.H. Adelson, "The Laplacian Pyramid as a Compact Image Code," *IEEE. Trans. Communications*, Vol. 31, pp. 532-540, 1983.
6. C.W.G. Clifford, K. Langley and D.J. Fleet, "Centre-Frequency Adaptive IIR Temporal Filters for Phase-Based Image Velocity Estimation," *Image Processing and its Applications*, Vol. 4-6, pp. 173-177, 1995.
7. I. Daubechies, *Ten Lectures on Wavelets*, Society for Industrial and Applied Mathematics, Philadelphia, 1992.
8. J. G. Daugman, "Complete Discrete 2-D Gabor Transforms by Neural Networks for Image Analysis and Compression," *IEEE Trans. Acoust., Speech, Signal Processing*, Vol. 36:7, pp. 1169-1179, 1988.
9. D.J. Fleet and A.D. Jepson, "Computation of Component Image Velocity from Local Phase Information," *International Journal of Computer Vision*, Vol. 5, pp. 77-104, 1990.
10. W.T. Freeman and E.H. Adelson, "The Design and Use of Steerable Filters," *IEEE Trans. on Pattern Analysis and Machine Intelligence*, Vol. 13:9, pp. 891-906, 1991.
11. M. Gökstorp and P-E. Danielsson, "Velocity Tuned Generalized Sobel Operators for Multiresolution Computation of Optical Flow," *IEEE*, pp. 765-769, 1994.
12. D.J. Heeger, "Optical Flow Using Spatiotemporal Filters," *International Journal for Computer Vision*, Vol. 1, pp. 279-302, 1988.

13. B.K.P Horn and B.G. Schunck, "Determining Optical Flow," *A.I. Memo No. 572, Massachusetts Institute of Technology*, 1980.
14. B.K.P Horn and B.G. Schunck, "Determining Optical Flow," *Artificial Intelligence*, Vol. 17, pp. 185-204, 1981.
15. B. Jähne, "Spatio-Temporal Image Processing," *Lecture Notes in Computer Science* vol. 751, Springer Verlag, 1993.
16. B. D. Lucas and T. Kanade, "An Iterative Image Registration Technique with an Application to Stereo Vision," *Proc. DARPA Image Understanding Workshop*, pp. 121-130, 1981.
17. S.G. Mallat, "A Theory for Multiresolution Signal Decomposition," *IEEE Trans. on Pattern Analysis and Machine Intelligence*, Vol. 11:7, pp. 674-693, 1989.
18. E.P. Simoncelli, W.T. Freeman, "The Steerable Pyramid: a Flexible Architecture for Multi-Scale Derivative Computation," *2nd Annual IEEE International Conference on Image Processing, Washington DC*, 1995.
19. A.B. Watson, "The Cortex Transform: Rapid Computation of Simulated Neural Images," *Computer Vision, Graphics, and Image Processing*, Vol. 39:3, pp. 311-327, 1987.
20. A.B. Watson and A.J. Ahumada, Jr, "Model of Human Visual-Motion Sensing," *Journal of Optical Society of America*, Vol. A:2-2, pp. 322-342, 1985.
21. J. Weber and J. Malik, "Robust Computation of Optical Flow in a Multi-Scale Differential Framework," *International Journal of Computer Vision, Vol. 14:1, pp. 5-19, 1995*